Transportation Research Part B 134 (2020) 210–228

Contents lists available at ScienceDirect

Transportation Research Part B

journal homepage: www.elsevier.com/locate/trb

Statistical inference for two-regime stochastic car-following models

Tu Xu, Jorge Laval*

School of Civil and Environmental Engineering, Georgia Institute of Technology, 790 Atlantic Dr NW, Atlanta, GA 30313, United States

ARTICLE INFO

Article history:
Received 19 October 2018
Revised 23 October 2019
Accepted 5 February 2020

Keywords:
Car-following model
Stochastic acceleration process
Stop-and-go traffic
Maximum-likelihood estimation

ABSTRACT

This paper presents the formulation of a family of two-regime car-following models where both free-flow and congestion regimes obey statistically independent random processes. This formulation generalizes previous efforts based on Brownian and geometric Brownian acceleration processes, each reproducing a different feature of traffic instabilities. The probability density of vehicle positions turns out to be analytical in our model, and therefore parameters can be estimated using maximum likelihood. This allows us to test a wide variety of hypotheses using statistical inference methods, such as the homogeneity of the driver/vehicle population and the statistical significance of the impacts of roadway geometry. Using data from two car-following experiments, we find that (i) model parameters are similar across repeated experiments within the same dataset but different across datasets, (ii) the acceleration error process is closer to a Brownian motion, and (iii) drivers press the gas pedal harder than usual when they come to an upgrade segment. Additionally, we explain the cause of traffic oscillations traveling downstream, which were observed both in the field data and in our simulations. The model is flexible so that newer vehicle technologies can be incorporated to test such hypotheses as differences in the car-following parameters of automated and regular vehicles, when data becomes available.

1. Introduction

Stop-and-go driving conditions (traffic oscillations) in traffic congestion increase not only financial costs and environmental pollution (Bilbao-Ubillos, 2008) but also the likelihood of car crashes (Zheng et al., 2010). Intensive research has been done on its contributing factors and properties. However, we still have limited knowledge about traffic oscillations. Mauch and Cassidy (2002), Laval (2005), Laval and Daganzo (2006), Ahn and Cassidy (2007) and Zheng et al. (2011) have demonstrated that lane changing is a major factor causing traffic oscillations and Sugiyama et al. (2008) showed that stop-and-go traffic can occur on a one-lane ring road without lane changing movements. A convincing explanation for this phenomenon is still lacking.

Several analytical studies have proposed that a small driving instability may grow into mature traffic oscillations in the absence of lane changing (Treiber et al., 1999; Wilson, 2008; Wilson and Ward, 2011; Treiber and Kesting, 2012; 2017). However, these models require either further model validation with empirical data or a careful selection of parameter values. On the other hand, Laval and Leclercq (2010), Chen et al. (2012a) and Chen et al. (2012b) argue that timid or aggressive car-

* Corresponding author.
E-mail address: jorge.laval@ce.gatech.edu (J. Laval).

https://doi.org/10.1016/j.trb.2020.02.003
0191-2615/

following behaviors caused the formation and propagation of traffic oscillations. These models are validated with empirical data, but they require at least four parameters that are not directly observable.

A more parsimonious family of car-following models, able to reproduce most traffic instabilities, is based on stochastic processes to describe drivers' desired accelerations. Laval et al. (2014) assume a constant standard deviation of driver acceleration, resulting in a Brownian motion (BM) process that explained realistic traffic oscillations with only one unobservable parameter. However, this model is unable to explain the decreasing relationship between queue discharge rate and the speed in the queue, as observed empirically in Yuan et al. (2015), and called "speed-capacity relationship" hereafter.

Yuan et al. (2018) argue that empirical data reveals that the standard deviation of the driver desired acceleration is not constant, as in the BM model, but decreases linearly with speed, leading to a geometric Brownian acceleration process. This geometric Brownian acceleration process successfully explains empirical speed-capacity relationships but does not produce periodic traffic oscillations. This paper aims to regulate the type of driver error on a scale from Brownian motion (BM) to geometric Brownian motion (g-BM) acceleration processes, and thus we can capture all said features of traffic instabilities.

The estimation of stochastic car-following model parameters has a short history because the vast majority of car-following models existing in the literature are deterministic. To the best of our knowledge, the only relevant reference would be Ahmed (1999) and Hoogendoorn and Ossen (2005), who use MLE for stochastic car-following models of the type:

$$x_j(t) = F(\mathbf{x}; \Theta) + \epsilon \tag{1}$$

where $x_j(t)$ is the vehicle position time t (or speed or acceleration), F is a deterministic car-following model with parameters $\Theta = (\theta_1, \theta_2, \ldots)$, $\mathbf{x}=\{x_j(t_i)\}$ are the trajectory data points for vehicle $j = 1, 2, \ldots$ at times $t_i, i = 1, 2, \ldots,$ and ϵ is a normal random variable with mean of zero and constant standard deviation. The problem with this formulation is that the additive error may not be appropriate for car-following models, which are generally accepted to be *two-regime* models, such as the one analyzed in this paper. These models recognize that the free-flow and congestion components obey completely different laws, which are reconciled under the minimum operator. It follows that a stochastic extension would *not be* an additive model. If random noises are to be added in such models, each regime should include errors of different nature and magnitudes, which would not be consistent with (1). In this paper, the probability density of vehicle positions turns out to be analytical. This means that we are not constrained by the additive error assumption of existing formulations, and model parameters will have better statistical properties.

The remainder of the paper is organized as follows. Section 2 presents a review of the formulation and features of the existing car following models based on stochastic acceleration process. Section 3 formulates the proposed model and analyzes its properties. Sections 4 and 5 estimate model parameters using maximum-likelihood estimation and test a wide variety of hypotheses using statistical inference methods. Section 6 analyzes the simulation results based on the extended desired acceleration model. Finally, Section 7 discusses conclusions and future work.

2. Background: Stochastic desired acceleration car-following framework

Car-following models based on stochastic desired acceleration models started with Laval et al. (2014). They generalize Newell's car-following framework (Newell, 2002) with bounded accelerations (Leclercq et al., 2007; Leclercq and Laval, 2007; Laval and Leclercq, 2008; 2010; Leclercq et al., 2011) by including a stochastic process to account for driver error during acceleration. It was found that this component is crucial for capturing realistic formation and propagation of traffic oscillations. The model can be expressed as:

$$x_j(t) = \min\{\underbrace{x_j(t-\tau) + \xi_j(\tau)}_{\text{free-flow}}, \underbrace{x_{j-1}(t-\tau) - \delta}_{\text{congestion}}\}, \tag{2}$$

where $x_j(t)$ is the position of j-th vehicle at time t, τ is the wave trip time between two consecutive vehicle trajectories and δ is the jam spacing. In this *two-regime* modeling framework the congestion term is deterministic while the free-flow term is stochastic. The $\xi_j(\tau)$ is a realization of the stochastic process describing the desired displacement of vehicle j during $t-\tau$ and t. This displacement is as a result of a stochastic desired acceleration model, which gives desired acceleration:

$$a = a(v), \tag{3}$$

that the driver imposes to the vehicle when traveling at speed $v(t)$ at time t under free-flow conditions, i.e., when unobstructed by the leading vehicle. The desired acceleration model captures both driver behavior and the physical limitations imposed by roadway geometry on the engine.

Based on empirical measurements, Laval et al. (2014) suggests the following linear model for the mean desired acceleration $\mathrm{E}[a(v)]$ under free-flow conditions:

$$\mathrm{E}[a(v)] = (v_c - v(t))\ \beta, \tag{4}$$

where $v(t)$ is the vehicle speed, v_c is the desired speed and β is the inverse relaxation time. (4) can be time-integrated twice to give

$$\mathrm{E}[\xi(t)] = v_c t - (1 - e^{-\beta t})(v_c - v_0)/\beta, \tag{5}$$

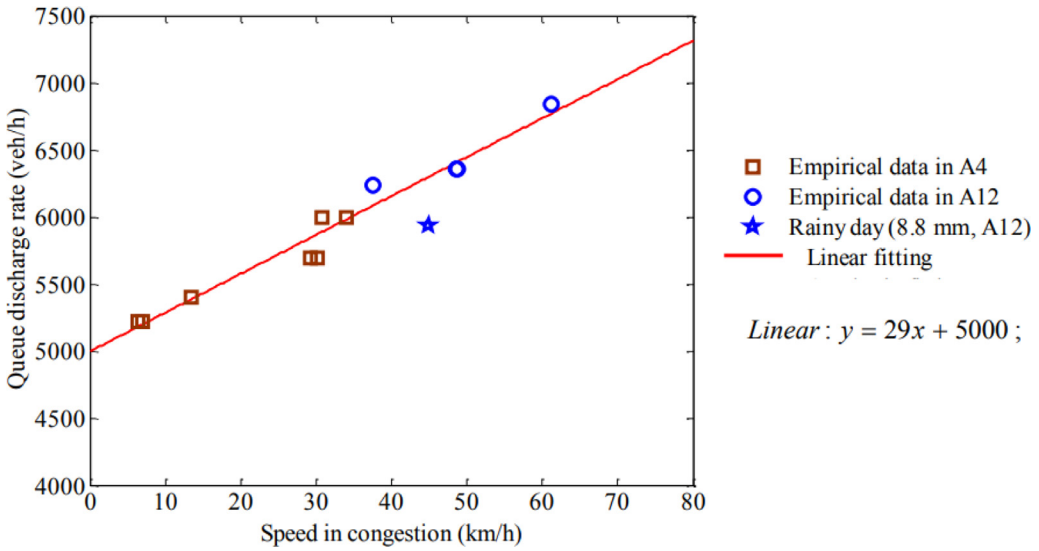

Fig. 1. Relation between queue discharge rate and the speed at the bottleneck. The data is collected on three-lane sections on two freeways in the Netherlands by Yuan et al. (2015).

The key to this modeling framework is the specification of the acceleration error around the mean desired vehicle acceleration E[$a(v)$], which has profound implications in the ability of the model to replicate traffic instabilities. Laval et al. (2014) assume that vehicle accelerations are normally distributed with a constant standard deviation, SD[$a(v)$], which gives the following BM stochastic differential equation:

$$\textbf{BM:}\begin{cases} d\xi(t) = v(t)dt, \qquad \xi(0) = 0, & (6a)\\ dv(t) = (v_c - v(t))\beta dt + \sigma dW(t), \qquad v(0) = v_0, & (6b)\end{cases}$$

where $W(t)$ is a standard BM and σ is its diffusion coefficient. This is probably the simplest model that captures (i) bounded accelerations due to gravity and (ii) produce realistic traffic oscillations (due to driver random errors while accelerating).

However, Yuan et al. (2018) observe that model (2)–(6) is unable to reproduce the speed-capacity relationship, as observed empirically in Yuan et al. (2015), shown in Fig. 1. Notice that the speed-capacity relationship is intimately related to the hysteresis phenomenon in traffic flow (Treiterer and Myers, 1974; Ahn et al., 2013; Chen et al., 2012b). Hysteresis refers to the discrepancy in the traffic states before and after a platoon of vehicles passes through a congested wave, were most of the time the deceleration phase exhibits higher flow than the acceleration phase (Laval, 2011). The speed-capacity relationship can be considered as a special case where the flow in the acceleration phase is related to the speed inside the congested wave. Based on the empirical data shown in Fig. 2, they argued that the standard deviation of the driver desired acceleration, SD[$a(v(t))$], is not constant but decreases linearly with the speed. Assuming that SD[$a(v(t))$] vanishes at v_c, the problem can be modeled as a g-BM, i.e.:

$$\textbf{g-BM:}\begin{cases} d\xi(t) = v(t)dt, \qquad \xi(0) = 0, & (7a)\\ dv(t) = (v_c - v(t))\beta dt + (v_c - v(t))\ \sigma\ dW(t), \qquad v(0) = v_0, & (7b)\end{cases}$$

Although model (2)-(5) and (7) was shown to reproduce the bottleneck discharge rate-speed in queue relationship, it loses the ability to produce realistic traffic oscillations as shown in Fig. 3. Here we argue that this is due to the error term vanishing at the desired speed, per (7b), which implies that at high speeds oscillations are not likely to form.

To implement these models and the one presented momentarily, one has to solve (6) and (7) to obtain the distribution $v(t)$ and $\xi(t)$. Then, we generate a realization of $\xi(t)$ and use it in the car-following model (2). Notice that $\xi(t) = \int_0^t v(s)ds$ tends to be normally distributed (by the Central Limit Theorem) all we need are the mean and variance of $\xi(t)$, which can be obtained analytically.

3. The proposed model

A general two-regime stochastic car-following model may be formulated as follows. Let the random process $X_j(t)$ represent the position of vehicle j at time t, and let $f(x;\ \Theta)$ be the probability density function of $X_j(t)$ given the set of model parameters $\Theta = (\theta_1, \theta_2, \ldots)$ and the data $\mathbf{x}$=$\{x_j(t_i)\}$, which represents the observed trajectories of all vehicles $j = 1, 2, \ldots$ at times $t_i, i = 1, 2, \ldots$ up to time t. According to (2) we write

$$X_j(t) = \min\{Y(\mathbf{x};\ \Theta), Z(\mathbf{x};\ \Theta)\} \qquad (8)$$

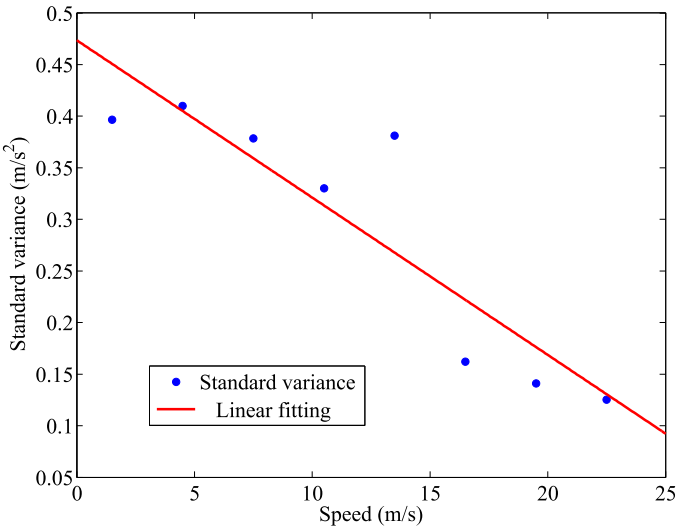

Fig. 2. Standard deviation of the desired accelerations in 5-m/s speed bins. A linear function $\mathrm{SD}[a(v(t))] = 0.015v(t) + 0.47$ is applied to fit the data. The data are from car-following experiments in Laval et al. (2014), collected when the test vehicle is the platoon leader stopped in front of a red signal.

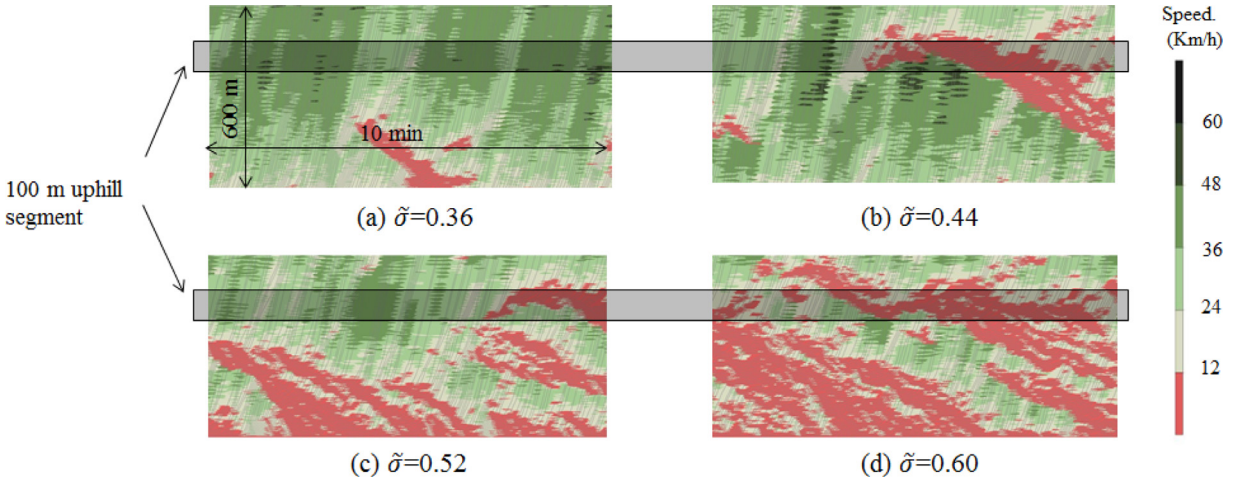

Fig. 3. Traffic patterns generated using g-BM model, showing the model's inability to generate realistic traffic oscillations despite the different model parameter values. The simulations were conducted on a 1-lane, 600m road segment with a 100m, 5 percent upgrade.

Since the desire to accelerate Y and the need to break Z obey completely different rules with different stimuli, we can safely assume that they are independent. In addition, if random processes Y and Z are normally distributed:

$$Y \sim N(\mu_Y, \sigma_Y), \qquad Z \sim N(\mu_Z, \sigma_Z)$$

where $\mu_{\_}$ and $\sigma_{\_}$ are the mean and standard deviation of the variable in subscript, one can show that (Nadarajah and Kotz, 2008):

$$f(x;\Theta) = \frac{1}{2\sqrt{2\pi}}\left(\frac{1}{\sigma_Z}e^{-\frac{(\mu_Z-x)^2}{2\sigma_Z^2}}\operatorname{erfc}\left(\frac{x-\mu_Y}{\sqrt{2}\sigma_Y}\right) + \frac{1}{\sigma_Y}e^{-\frac{(\mu_Y-x)^2}{2\sigma_Y^2}}\operatorname{erfc}\left(\frac{x-\mu_Z}{\sqrt{2}\sigma_Z}\right)\right) \tag{9}$$

where $\operatorname{erfc}(x) = \frac{2}{\sqrt{\pi}}\int_x^\infty e^{-t^2}\,dt$ is the complementary error function. This result is notable because the model is analytical and lends itself nicely to be estimated using MLE. In addition, it should have a much better explanatory power compared to existing models that are additive such as (1).

3.1. The congestion term

Based on our previous discussion, it is advantageous to consider both the free-flow (Y) and the congestion (Z) terms normally distributed, as opposed to the original model (2) where Z is deterministic. As demonstrated empirically in

Ahn et al. (2003) parameters τ and δ can be assumed to follow the bivariate normal (BVN) distribution (Ahn et al., 2003), i.e.

$$(\tau, \delta) \sim BVN(\mu_\tau, \mu_\delta, \sigma_\tau, \sigma_\delta, \rho).$$

Instead of taking the parameters directly from Ahn et al. (2003), here we estimate them in conjunction with the free-flow regime parameters, which are formulated next.

3.2. The free-flow term

We start by rewriting the proposed car-following model (2)–(7) as:

$$X_j(t) = \min\{\underbrace{x_j(t-\tau') + \xi_j(\tau')}_{\text{free-flow (Y)}}, \underbrace{x_{j-1}(t-\tau) - \delta}_{\text{congestion (Z)}}\}, \tag{10}$$

to emphasize that the time lag in free-flow, τ', and in congestion, τ, do not have to be the same, as customary in the literature, and should be statistically independent. Furthermore, we argue that τ' should not be interpreted as a parameter because it simply defines the initial conditions for the free-flowing component. For simplicity, we fix the value of τ' in the parameter estimation process to

$$\tau' = 1.2s,$$

which is a typical value for the time step in Newell-type car-following models, but any comparable value could be used instead. The main ingredients of the free-flow regime formulation is the displacement ξ_j, as explained next.

3.2.1. The extended desired acceleration model

Section 2 showed that there is a trade-off between the specification of the acceleration error (i.e, BM or g-BM) and the traffic feature that can be replicated (i.e., realistic traffic oscillations or speed-capacity relationship). In this paper, we introduce a single extra dimensionless parameter $m \geq 1$, that produces models in a scale from the g-BM model ($m = 1$) to the BM model ($m >> 1$), and therefore generalizes the models in the previous section; see Fig. 4. The hope is that a suitable value of m will produce a model with the best features of the BM and g-BM models, namely:

1. realistic traffic oscillations: the BM model produces traffic oscillations even at high speeds because the acceleration error SD[$a(v(t))$] is independent of the speed. In contrast, the g-BM model cannot because the SD[$a(v(t))$] is assumed to be zero at the desired speed v_c.
2. speed-capacity relationship: the g-BM model reproduces this relationship because SD[$a(v(t))$] is a decreasing function of the speed. In contrast, the BM model cannot because SD[$a(v(t))$] is assumed constant.

Based on these observations, we conjecture that the acceleration error SD[$a(v(t))$] has to be nonzero at v_c and be a decreasing function of the speed. Here, we impose that SD[$a(v(t))$] vanish at mv_c and the stochastic differential equation for the proposed acceleration model becomes:

$$\begin{cases} d\xi(t) = v(t)dt, \quad \xi(0) = 0, & \text{(11a)} \\ dv(t) = (v_c - v(t))\beta dt + (mv_c - v(t))\sigma dW(t), \quad v(0) = v_0, & \text{(11b)} \end{cases}$$

and has analytical solution. For the car-following implementation we simply generate $\xi(t)$ as a normal random variable with mean E[$\xi(t)$] given by (5) and Var[$\xi(t)$] shown in Appendix A.

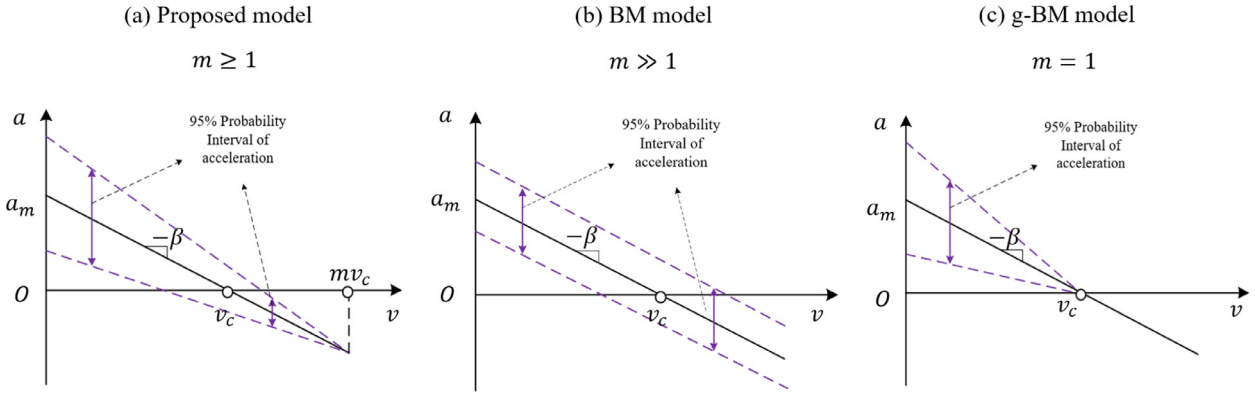

Fig. 4. Desired acceleration models. In the proposed model the standard deviation of the desired acceleration decrease linearly with the vehicle speed, but does not vanish at v_c. The region between two purple lines represents the 95% probability interval of accelerations.

As mentioned previously, the parameter m can be interpreted as a knob that regulates how close the model is to the BM or g-BM models. When $m = 1$, it can be seen immediately from (11b) that the proposed model is equivalent to the g-BM car-following model. When $m >> 1$, the model is equivalent to the BM model. To see this, notice that

$$\frac{\mathrm{SD}[a(v)]}{\mathrm{SD}[a(0)]} = \frac{(mv_c - v)\sigma\, dW(t)}{(mv_c - 0)\sigma\, dW(t)} = 1 - \frac{v}{mv_c}. \tag{12}$$

A reasonable vehicle speed v is usually greater than 0 and smaller than $2v_c$, so we have $0 < \frac{v}{v_c} < 2$. Along with $m >> 1$, we have $1 - \frac{v}{mv_c} \approx 1 - 0 = 1$, and thus we can say that the driver error, $\mathrm{SD}[a(v(t))]$, is constant in terms of vehicle speed, and therefore the acceleration process is a BM.

3.2.2. Physical bounds on the parameters $m, \tilde{\sigma}$

As with any normally distributed random variable there is always a probability that it will be negative. Following Laval et al. (2014), for the worst case scenario $v(0) = 0$, we need $P\{\tilde{v}(\beta\tau) \le 0\} \le \alpha$, for a small prescribed α. For typical values $\beta \approx 0.07\mathrm{s}^{-1}$ and $\tau \approx 1.2\mathrm{s}$ and $\alpha = 0.05$, one has:

$$m\tilde{\sigma} \le 0.2$$

is a secure range of parameter values for the acceleration process starting from a complete stop. If a negative speed is realized in the simulation, it should be set to 0.

Here, $m\tilde{\sigma} \le 0.2$ is the secure range of parameters during an acceleration process from a complete stop, i.e. $v(0) = 0$. For usual cases, for example when $v(0) = 60$ km/h, the bound of the product of two parameters could be much higher because $v(\beta\tau) \le 0$ is very unlikely to happen.

3.2.3. Formulation with roadway upgrade

To take the upgrade of the roadway into account, we replace (4) by

$$\mathrm{E}[a(v)] = (u - v(t))\ \beta + \alpha g \max\{0, G\}, \tag{13}$$

where u is the free-flow speed, i.e. the desired speed on a flat road segment, $g = 9.81$ m/s^2 is the acceleration of gravity, G is the roadway grade expressed as a decimal and α is a dimensionless parameter. Notice that in the literature $\alpha = -1$, which is consistent with the assumption that the acceleration due to gravity in the direction of movement, $g\max\{0, G\}$, is subtracted, in its entirety, from the acceleration the driver would impose to the vehicle on a flat segment, $(v_c - v(t))\ \beta$. Here, we add the parameter α to relax this strong assumption in the literature: $\alpha > -1$ indicates they compensate for the upgrade, i.e. that they press the gas pedal harder than they would on a flat segment, while $\alpha < -1$ implies a softer than usual pressing. Values of $\alpha > 0$ are unlikely as it would indicate that acceleration increases with the upgrade

Notice that the desired speed becomes a function of the upgrade, and can be expressed as:

$$v_c = u + \alpha g \max\{0, G\}/\beta. \tag{14}$$

3.2.4. Dimensionless formulation

In this section we formulate the proposed model in a dimensionless form to identify a the key parameters that drive the model. One possibility is the following transformations:

$$\tilde{t} = \beta t, \qquad \tilde{v}(\tilde{t}) = v(\tilde{t})/v_c, \qquad \tilde{\xi}(\tilde{t}) = \beta\xi(\tilde{t})/v_c, \qquad \tilde{\sigma}^2 = \sigma^2/\beta. \tag{15}$$

where dimensionless variables are indicated with a tilde. It follows that the dimensionless form of (11) is:

$$\begin{cases} \tilde{\xi}(\tilde{t}) = v(\tilde{t})dt, \quad \tilde{\xi}(0) = 0, & \text{(16a)} \\ \tilde{v}(\tilde{t}) = (1 - \tilde{v}(\tilde{t}))d\tilde{t} + (m - \tilde{v}(\tilde{t}))\tilde{\sigma}\, dW(\tilde{t}), \quad \tilde{v}(0) = v_0/v_c, & \text{(16b)} \end{cases}$$

It can be seen that besides the initial conditions $\tilde{\xi}(0)$ and $\tilde{v}(0)$, the only two non-observable parameters that drive this model are m and $\tilde{\sigma}$. The estimation of these parameters will be carried out in Section 4.

3.2.5. Speed-Capacity relationship in congestion

Here we show how the new parameter m influences the speed-capacity relationship predicted by our model. Toward that end, we simulate a 25-car following experiment on a one-lane road with different speed in congestion and different values of model parameters. The vehicles initially travel at a speed lower than free-flow speed in congestion and then accelerate to free-flow speed. The discharge rate is measured at the place where the second vehicle reaches free-flow speed. A sample trajectory of the experiment is provided in Fig. 5.

Fig. 6 plots the results. It can be seen that for $m < 2$ the model captures the speed-capacity relationship consistently with the empirical data in Yuan et al. (2015). But as the value of m increases, the model gradually loses its ability to capture this relationship.

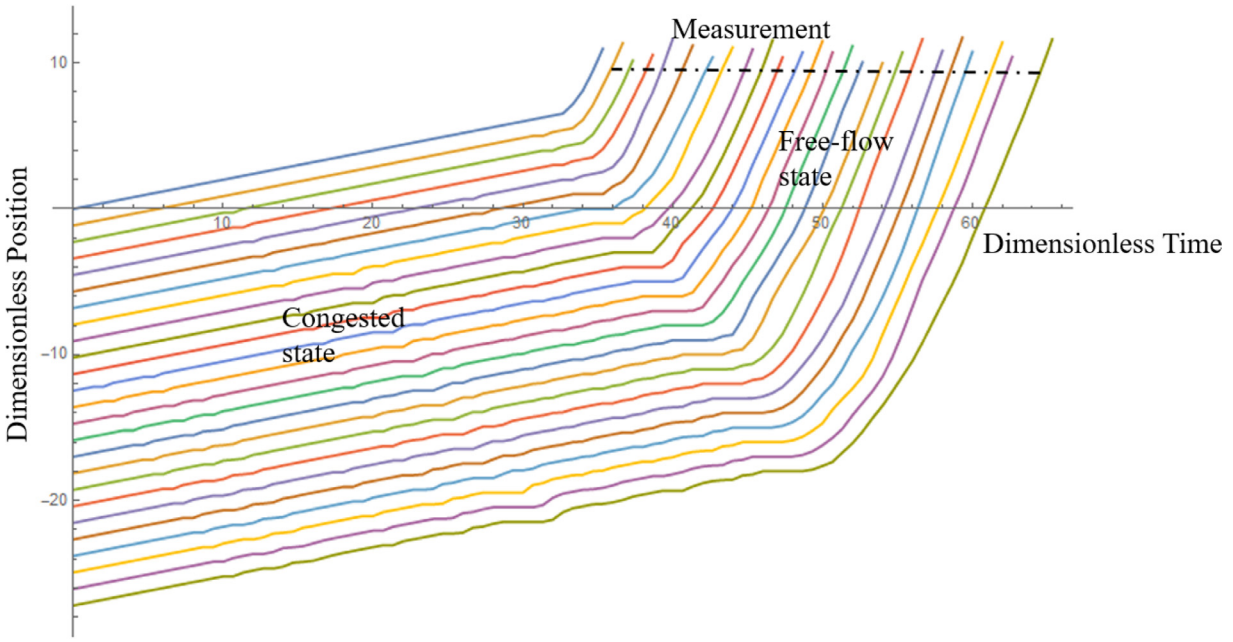

Fig. 5. Sample trajectories of the queue discharge experiment with $\tilde{v_0} = 0.1$, $m = 1.25$ and $\tilde{\sigma} = 0.35$. The initial spacing of the vehicles is in equilibrium and calculated based on the congested branch of the triangular fundamental diagram $\delta + \tilde{v_0}\tau$. The discharge rate is measured at the black dash line where the speed of the second vehicle reaches free flow speed.

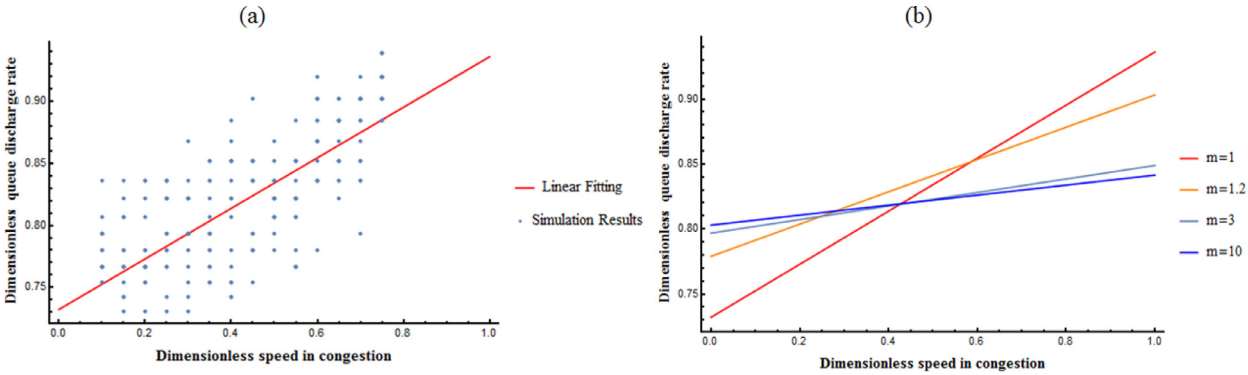

Fig. 6. (a) Simulation results and a linear fitting of the desired model with parameter $m = 1$, which shows a positive relationship between queue discharge rate and speed in congestion. (b) Dimensionless queue discharge rate as a function of dimensionless speed in congestion for $m \in \{1, 1.2, 3, 10\}$. The model gradually loses its ability to catch the positive relationship between speed and queue discharge rate with the increase of the value of m.

4. Estimation of model parameters

In this section, we apply maximum-likelihood estimation (MLE) to estimate the parameters in our proposed model (10). Based on the formulation in the previous section, it is not difficult to show that the mean and variance of the free-flow term ($Y = x_j(t - \tau') + \xi_j(\tau')$) and congestion term ($Z = x_{j-1}(t - \tau) - \delta$) are given by:

$$\begin{cases} \mu_Y = x_j(t - \tau') + \mathrm{E}\big[\xi(\tau')\big], & \text{(17a)} \\ \sigma_Y^2 = \mathrm{Var}\big[\xi(\tau')\big], & \text{(17b)} \\ \mu_Z = x_{j-1}(t - \mu_\tau) - \mu_\delta - a_{j-1}(t - \mu_\tau)\sigma_\tau^2/2, & \text{(17c)} \\ \sigma_Z^2 = v_{j-1}^2(t - \mu_\tau)\sigma_\tau^2 + \sigma_\delta^2 + 2\rho v_{j-1}^2(t - \mu_\tau)\sigma_\tau\sigma_\delta, & \text{(17d)} \end{cases}$$

which is all we need to evaluate (9). In (17a) and (17b) recall that $\tau' = 1.2$s is a constant, and that $\mathrm{E}[\xi(t)]$ is given in (5) and $\mathrm{Var}[\xi(t)]$ in Appendix A. For (17c) and (17d) we used second- and first-order approximations (Ang and Tang, 2007) for $\mathrm{E}\big[x_{j-1}(t - \tau) - \delta\big]$ and $\mathrm{Var}\big[x_{j-1}(t - \tau) - \delta\big]$, respectively, and $a_{j-1}(t)$ is the acceleration of vehicle $j - 1$ at time t.

Before we can use MLE to estimate the parameters:

$$\Theta = (\mu_\tau, \mu_\delta, u, \beta, m, \tilde{\sigma}, \rho, \sigma_\tau, \sigma_\delta, \alpha)$$

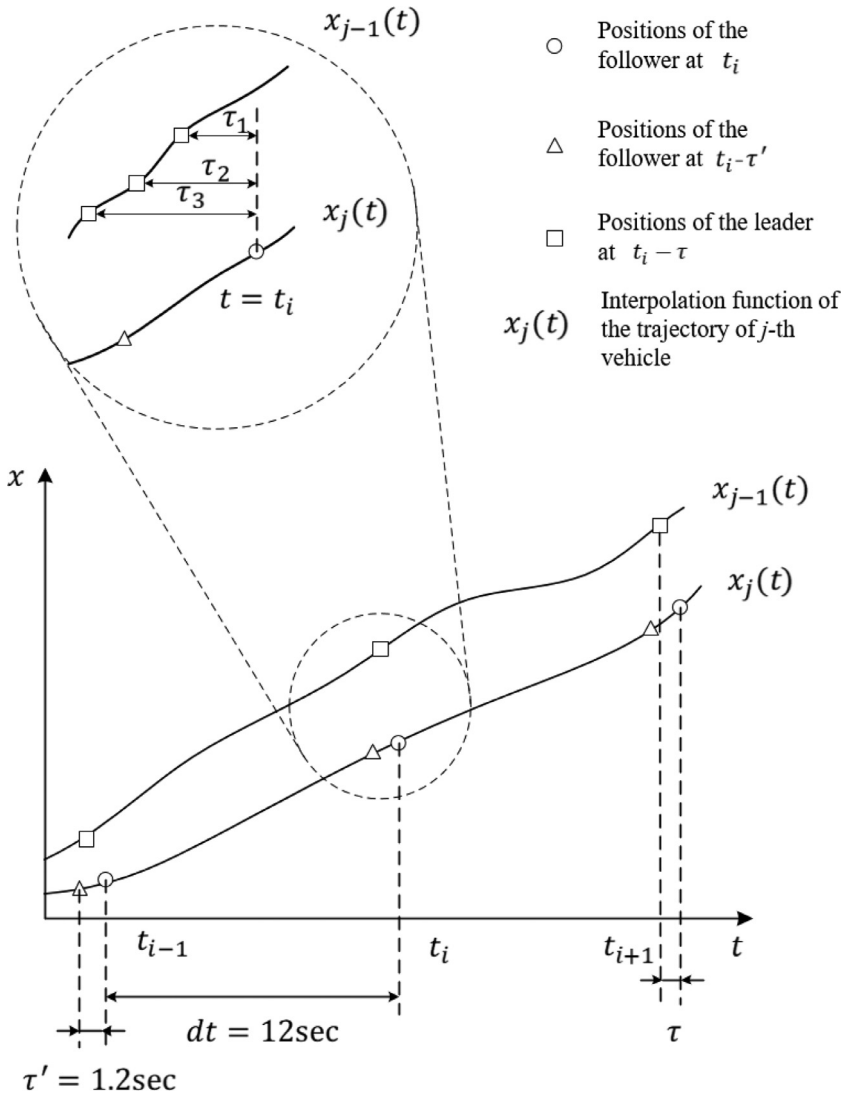

Fig. 7. Key aspects for maximum likelihood estimation. In this figure, $x_j(t)$ represents the interpolated trajectory of vehicle j. To perform the maximum likelihood estimation, we first choose discrete times t_1, t_2, ..., t_i, ... as our data $\mathbf{x}$. Then for each time t_i, the circle represents the observed position of vehicle j at t_i, the triangle represents the observed position of vehicle j at time $(t_i - \Delta t)$, and the square represents the observed positions of vehicle $j-1$ at time $(t_i - \tau)$. The zoomed in figure shows that the positions of squares are not fixed but depend on the value of the random variable τ. The uncertainty of the position of the squares indicates the randomness of parameter τ.

we perform two additional steps. First, we constrain the parameter search space within the upper and lower bounds shown in Table 1, to ensure that the estimation results remain physically meaningful and to avoid spurious local maxima.

Secondly, we perform a third-order interpolation on the discrete trajectory data so that the $x_j(t)$, its derivative $v_j(t)$ and its second derivative $a_j(t)$ become continuous functions of time. This is illustrated in Fig. 7, where at times $\{t_1, t_2, ...t_i, ...\}$, we have $\mathbf{x} = \{x_j(t_1), x_j(t_2), ...x_j(t_i), ...\}$ represented by circles, the $\{x_j(t_1 - \tau'), x_j(t_2 - \tau'), ...x_j(t_i - \tau'), ...\}$ in (17a) represented by triangles and the $\{x_{j-1}(t_1 - \mu_\tau), x_{j-1}(t_2 - \mu_\tau), ...x_{j-1}(t_i - \mu_\tau), ...\}$ in (17c) represented by squares. The randomness of parameter τ is shown by the uncertainty of the position of the squares on Fig. 7.

4.1. Data

We have two independent datasets for the parameter estimation.

Dataset 1: Jiang et al. (2014) conduct a car-following experiment with 25 vehicles all equipped with data collection devices. In this experiment, the vehicle platoon traveled northbound and southbound repeatedly, on a two-way 3.5 km suburban road segment in Hefei, China. An example of trajectory data is provided in Fig. 8. The grade data is also contained in the dataset.

Table 1
Upper and lower bounds for parameter estimation.

Parameter	Lower bound	Upper bound
μ_τ	0.4	2.0
μ_δ	3	20
u	60	90
β	50	350
m	1	10
$\tilde{\sigma}$	0	0.3
ρ	−1	1
σ_τ	0	1
σ_δ	0	5
α	−4	2

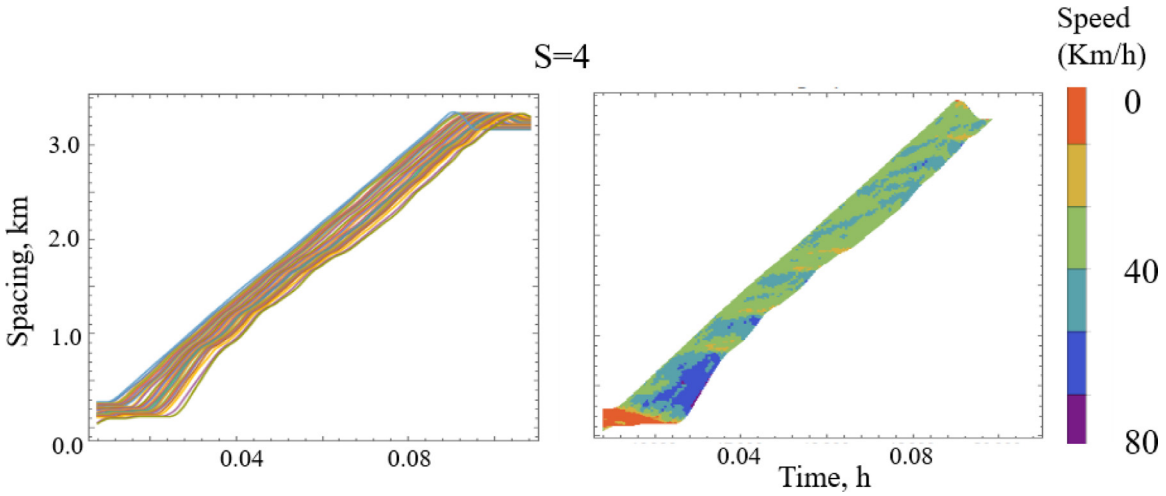

Fig. 8. An example of the trajectory data collected in a series of car-following experiments (Jiang et al., 2014). S=4 represents the ordinal number of the experiment.

Dataset 2: The second dataset is from Laval et al. (2014) who perform a similar car-following experiment on a two-lane road near Georgia Tech with six vehicles. The grade data is also provided.

In both two sets of experiments, the lead vehicle was instructed to maintain a given constant speed while other vehicles were expected to follow its leader naturally. There was no interference from traffic signals or other vehicles in the experiments.

Fig. 8 shows a typical car-following experiment, with the lead vehicle maintaining a constant low speed. Notice that the followers travel at speeds higher than the lead vehicle speed occasionally, as seen by the blue region in the figure, which is possible because the leader speed is much lower than the free-flow speed u.

5. Estimation results and statistical inference

Here we present the MLE parameters using all the data within each data set, and also for each particular experiment within each data set.

We randomly choose five car-following experiments from dataset 1. For each car-following experiment, we select a data point $x_j(t_i)$ each $dt = 12$ sec during a five-minute period for the first 15 cars such that 25 data points are used for each car and 375 data points are used in each car-following experiment. We perform MLE for each car-following experiment and also for the overall dataset ($375 \times 5 = 1875$ data points are used in total). For dataset 2, we used the same method for the six-vehicle platoon with a smaller $dt = 8$ sec during a 140-second period. 18 data points are used for each vehicle and $18 \times 5 = 90$ data points are used in each car-following experiment. $90 \times 5 = 450$ data points are used for the estimation of the overall dataset. We decreased the value of dt for dataset 2 in order to obtain more sample points without sacrificing independence. We tested different values of dt and find that the correlation among data points are negligible with the chosen dt. The parameter evaluation results for the overall datasets are provided in Table 2 and the results for each car-following experiments are listed in Table 3 and Table 4.

Parameters u and β are two major parameters in the free-flow branch, which determine the mean of the vehicle acceleration and ξ. The estimation results of u and β for both datasets have high statistical significance. These two variables are both significant. The free-flow speed u in dataset 2 is slightly higher than in dataset 1. The maximum acceleration $u\beta$ represents the desired acceleration when is at rest. A quick calculation tells us $u\beta$ in dataset 2 are approximately twice that in

Table 2
MLE parameter values for the overall datasets.

Parameter	Dataset 1		Dataset 2	
	Mean value	t-stat	Mean value	t-stat
$\widehat{\mu_\tau}$	0.63	10.4	0.47	3.5
$\widehat{\mu_\delta}$	4.87	11.0	4.38	2.5
$\widehat{u}$	64.1	7.9	67.9	23.1
$\widehat{\beta}$	66.5	9.7	210.4	7.1
$\widehat{m}$	4.9	10.6	5.0	2.2
$\widehat{\tilde{\sigma}}$	0.052	11.9	0.041	2.1
$\widehat{\rho}$	−0.7	−15.5	−0.6	−2.8
$\widehat{\sigma_\tau}$	0.48	22.5	0.12	2.9
$\widehat{\sigma_\delta}$	2.17	37.7	3.98	3.8
$\widehat{\alpha}$	−0.59	−12.3	−0.56	-5.3

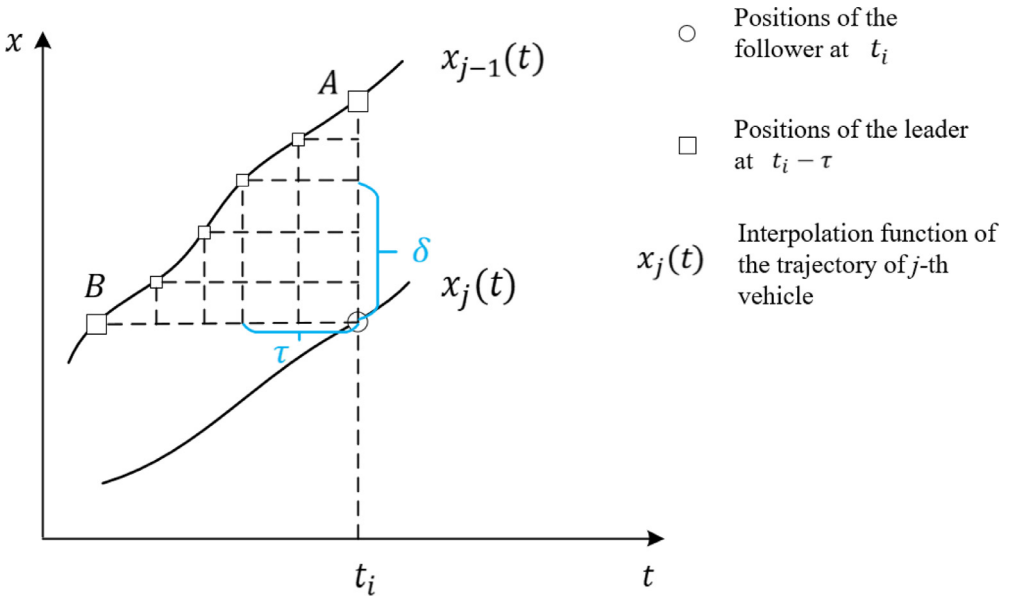

Fig. 9. This figure helps us understand the negative correlation between τ and δ. Note that all feasible (τ, δ) pairs give points on segment AB. Moving along this segment one can see that if τ increases then δ decreases and vice-versa.

dataset 1, indicating the vehicles in dataset 2 have much larger acceleration at rest than those in dataset 1. This result might be explained because in dataset 1 the lead vehicle is controlled to be traveling at a low speed near 30 km/h while leaders in dataset 2 are traveling at higher speeds. Parameters m and $\tilde{\sigma}$ determine the stochastic term in the free-flow branch. We have $m >> 1$ for both two datasets with high t-statistic and this indicates the driver acceleration process is closer to BM according to (12).

Parameters τ and δ are the key parameters controlling the congested branch in the model. Both μ_τ and μ_δ are statistically significant variables for the overall model given the high t-statistic. A typical value of τ would be around 1.2s and that of δ would be 7m. However, the estimated values of τ and δ are much smaller than the typical values, which means the vehicles in both datasets follow its leader closer than that in a typical vehicle platoon. We also find that τ and δ are negatively correlated because the estimated values of ρ are both less than 0 for both datasets and with high t-statistic. As can be seen in Fig. 9, this is as expected because all feasible (τ, δ) pairs give points on segment AB, and moving along this segment one can see that if τ increases then δ decreases and vice-versa.

Next, we take advantage of the statistical inference tools made possible by MLE to test several interesting hypotheses.

5.1. BM or g-BM?

Recall that we obtained high values of m in the estimation. Here we present the 95%-confidence intervals (CIs) of parameter m to test the hypotheses that $m = 1$. As we can see from Table 5, $m = 1$ is contained in three of these CIs so we cannot reject the null hypothesis $H_0 : m = 1$ in these three cases. However, the CIs of parameter m in most experiments strongly indicate that $m > 1$. Given the estimated mean value and CIs of m, one can see that the acceleration process is closer to BM than g-BM.

It can be seen that these CIs are fairly wide, and could be narrowed by increasing the sample size.

Table 3
MLE parameter values for dataset 1.

Experiment	$\widehat{\mu_\tau}$		$\widehat{\mu_\delta}$		$\hat{u}$		$\hat{\beta}$		$\hat{\bar{m}}$		$\hat{\bar{\sigma}}$		$\hat{\rho}$		$\widehat{\sigma_\tau}$		$\widehat{\sigma_\delta}$		$\hat{\alpha}$		log likelihood
	Mean	t-stat	Mean	t-stat	Mean	t-stat	Mean	t-stat	Mean	t-stat	Mean	t-stat	Mean	t-stat	mean	t-stat	mean	t-stat	mean	t-stat	
1	0.6	7.9	5.2	8.6	62.1	5.0	75.1	7.3	7.4	3.0	0.03	2.7	-0.7	-2.7	0.5	1.6	1.8	0.9	-0.7	-2.9	2514
2	0.7	3.7	5.5	4.7	61.9	14.2	69.2	15.1	6.3	2.6	0.04	2.1	-0.7	-0.9	0.5	3.2	1.6	0.6	-0.6	-3.5	2456
3	0.6	4.8	5.3	5.2	67.9	7.0	106.8	5.7	4.4	5.9	0.05	4.4	-0.7	-11.3	0.4	11.2	2.4	17.2	-1.0	-7.7	2361
4	0.6	3.1	4.7	3.3	61.9	3.9	83.3	5.3	7.6	4.7	0.03	14.1	-0.8	-4.4	0.3	2.9	1.9	6.6	-0.6	-2.2	2405
5	0.6	2.9	5.5	3.9	61.9	9.5	76.3	8.0	5.6	4.7	0.04	3.7	-0.9	-4.8	0.3	1.4	2.0	1.7	-0.6	-3.7	2465
Overall	0.6	10.4	4.9	11.0	64.1	7.9	66.5	9.7	4.9	10.6	0.05	11.9	-0.7	-15.5	0.5	22.5	2.2	37.7	-0.6	-11.7	12176

Likelihood-ratio test statistic $\Lambda(\mathbf{x}) = 50 < 56 = \chi^2(0.95, 40)$.

Table 4
MLE parameter values for dataset 2.

Experiment	$\widehat{\mu_\tau}$		$\widehat{\mu_\delta}$		$\widehat{u}$		$\widehat{\beta}$		$\widehat{\bar{m}}$		$\widehat{\bar{\sigma}}$		$\widehat{\rho}$		$\widehat{\sigma_\tau}$		$\widehat{\sigma_\delta}$		$\widehat{\alpha}$		log likelihood
	Mean	t-stat	Mean	t-stat	Mean	t-stat	Mean	t-stat	Mean	t-stat	Mean	t-stat	Mean	t-stat	mean	t-stat	mean	t-stat	mean	t-stat	
1	0.6	3.0	6.5	5.4	64.4	5.3	262.0	2.5	4.3	2.1	0.05	2.1	-0.7	-1.8	0.3	0.8	2.8	2.8	-0.6	-3.8	532
2	0.6	2.7	6.1	3.4	68.1	13.4	201.1	4.2	3.7	3.7	0.05	2.9	-0.6	-0.9	0.3	1.3	2.0	1.2	-0.9	-3.6	563
3	0.4	2.2	4.2	2.7	69.8	10.0	225.7	4.6	9.1	3.6	0.02	2.5	-0.7	-2.8	0.2	0.6	2.5	0.4	-0.5	-2.4	555
4	0.5	2.8	4.5	7.8	67.1	8.7	227.8	2.2	5.1	2.8	0.05	2.0	-0.7	-1.8	0.4	4.3	2.5	0.6	-0.6	-3.6	530
5	0.5	6.8	6.7	3.4	79.1	17.0	259.2	4.4	3.4	2.2	0.05	2.2	-0.7	-0.6	0.3	1.2	2.5	1.5	-0.8	-2.9	547
Overall	0.5	3.5	4.4	2.5	67.9	23.1	210.4	7.1	5.0	2.2	0.04	2.1	-0.6	2.8	0.1	2.9	4.0	3.8	-0.6	-5.3	2715

Likelihood-ratio test statistic $\Lambda(\mathbf{x}) = 24 < 56 = \chi^2(0.95, 40)$.

Table 5
95%-CIs of m for each car-following experiment.

Experiment	Dataset 1		Dataset 2	
	lower bound	upper bound	lower bound	upper bound
1	2.6	12.1	0.2	8.4
2	1.5	11.1	1.7	5.7
3	3.0	5.9	4.2	14.1
4	4.4	10.7	1.5	8.7
5	3.3	8.0	0.4	6.5
Overall	4.0	5.8	0.6	9.5

Table 6
95%-CIs of α for each car-following experiment.

Experiment	Dataset 1		Dataset 2	
	Lower bound	Upper bound	Lower bound	Upper bound
1	−1.2	−0.2	−0.9	−0.3
2	−1.0	−0.3	−1.4	−0.4
3	−1.2	−0.7	−1.0	−0.1
4	−1.2	−0.1	−1.0	−0.3
5	−0.9	−0.3	−1.4	−0.3
Overall	−0.7	−0.5	−0.8	−0.4

5.2. Are parameters different across datasets?

Here we test parameter homogeneity across datasets by performing likelihood-ratio tests. The methodology is summarized in Appendix B. If we estimate the parameters for each dataset, we have $n_1 = 2 \times 10 = 20$ parameters. If we estimate the parameters for two datasets combined, we have $n_2 = 10$ parameters. The chi-square critical value is $\chi^2(0.95, n_1 - n_2) = \chi^2(0.95, 10) = 18$. We have $\Lambda(\mathbf{x}) = 2\left[\ell(\mathbf{x}; \widehat{\Theta_1}) - \ell(\mathbf{x}, \widehat{\Theta_2})\right] = 2((12176 + 2715) - 13808)) = 2166 > 18$. This means we cannot accept the null hypothesis that the model with n_1 parameters has similar goodness-of-fit as the model with n_2 parameters. In other words, we cannot use unified parameter values for these two datasets. This result might be explained given that the values of β are significantly different across the two datasets.

5.3. Are parameters different across experiments?

Here we test parameter homogeneity across car-following experiments by performing likelihood-ratio tests. If we estimate parameter values for each experiment, we have $n_1 = 5 \times 10 = 50$ parameters. If we estimate parameter values for the overall dataset, we have $n_2 = 10$ parameters. Therefore, the chi-square critical value is $\chi^2(0.95, n_1 - n_2) = \chi^2(0.95, 40) = 56$. We have $\Lambda_1(\mathbf{x}) = 50 < 56$ for dataset 1 and $\Lambda_2(\mathbf{x}) = 24 < 56$ for dataset 2. This means we accept the null hypothesis that the model with n_1 parameters has similar goodness-of-fit as the model with n_2 parameters.

5.4. Should grade data be included in the model?

Here we discuss the importance of the grade in the model by testing the significance of parameter α in the model. The estimation results of α were shown in Table 3 for the overall models and in 4 for the individual experiments, giving the strong indication that this parameter is very significant in all cases. The fact that in all cases $-0.5 \leq \hat{\alpha} \leq -1$ reveals that drivers tend to compensate for the upgrade, as explained in Section 3.2.2, and that the current assumption in the literature that $\alpha = -1$ might not be warranted.

To take a closer look, the 95%-confidence intervals (CIs) of α are shown in Table 6. It can be seen that the upper bounds are all negative, which is reassuring of the fact that upgrades have a detrimental effect on acceleration. That some lower bounds are < -1 is problematic, as it indicates that some drivers might press the gas pedal softer than they would on level terrain, which is counterintuitive. However, this only happens in individual experiments where the reduced sample size might be to blame. In fact, the overall models exhibit upper and lower bounds that are very reasonable.

6. Simulations and oscillations propagating downstream

In this section, we conduct simulations with the proposed model. A comparison between the simulation results and field data is also presented.

For each vehicle in the simulation, we randomly generate τ_j and δ_j for 25 cars based on the estimated mean and standard error values from dataset 1. In the simulation, we input the leader trajectory from dataset 1 and then generate initial

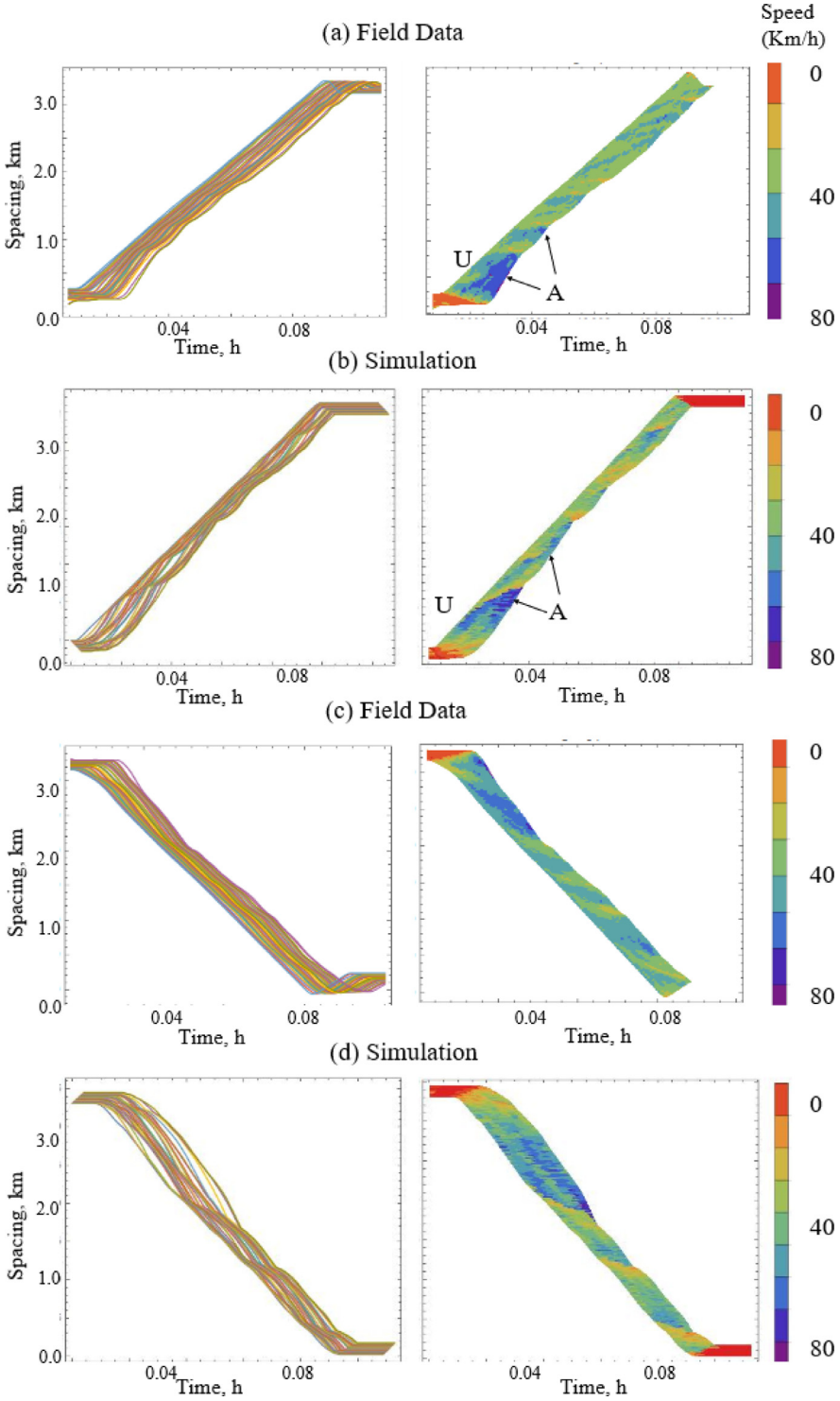

Fig. 10. A comparison between field trajectory data and simulation results. (a) Trajectories of a northbound car-following experiment; (b) simulation of the experiment in (a); (c) trajectories of a southbound car-following experiment; (d) simulation of the experiment in (c). The low-speed areas are identified in red or yellow, while high-speed areas are identified in purple or blue. We can observe the high resemblance between real trajectories and simulation results. In the figures, we can observe different traffic states U and A which will be explained next and shown in Fig. 11.

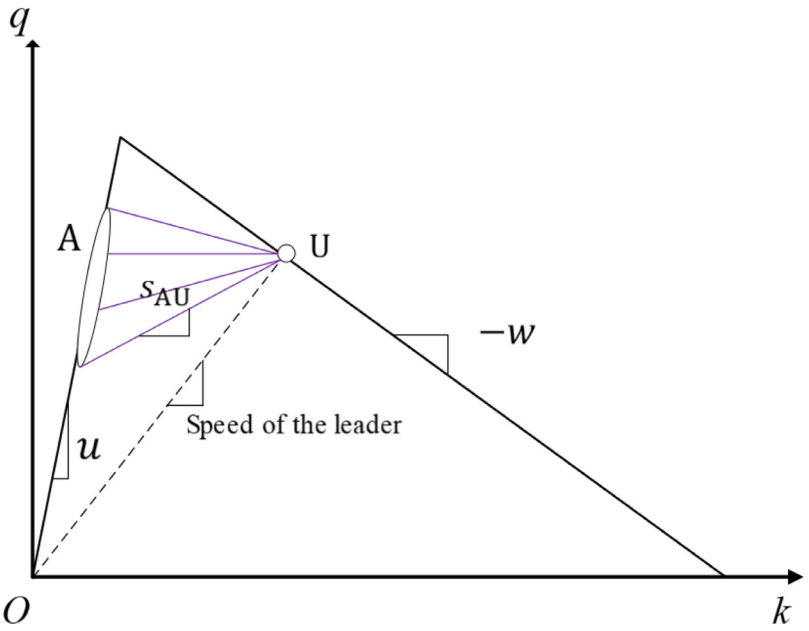

Fig. 11. The triangular fundamental diagram used to analyze the unusual wave speed and the trajectory bounces. The ellipse represents the possible positions of traffic state A. The purple lines represents the possible traffic shock waves with negative or positive wave speed.

conditions of the platoon based on parameters τ_j and δ_j. Given the estimated parameter values from dataset 1 and the initial conditions, we generate vehicle trajectories one by one with the model (8) - (17). The results are shown in Fig. 10.

In Fig. 10, we can see that the simulation results and the real data show high resemblance. The high-speed regions in the experiments occur at similar places in the simulations. Besides, we can observe oscillation propagating downstream and trajectories that "bounce" at the end of the vehicle-platoon in both field data and simulation results, as explained next.

It is well-known that traffic oscillations in congested traffic propagate upstream at the wave speed of approximately 20 km/hr. To our surprise, however, dataset 1 exhibits oscillation that travel downstream, and this phenomenon also occurs in our simulation results; see Fig. 10.

To explain this, recall that the driver acceleration process is a stochastic process, where some drivers would appear to accelerate more aggressively than others. As a result, large spacing will appear between leaders that are more aggressive than their followers, which can lead to low-density traffic states in the platoon. Let "A" denote these free-flow states where vehicles have the possibility of accelerating to speeds close to the free-flow speeds; see Figs. 10 and 11. Notice that these "pockets" of free flow inside congestion have been observed empirically in Kim and Cassidy (2012). Eventually, these vehicles will catch up to the leader traveling at a nearly constant speed and inducing congested traffic states "U" in Fig. 11. As a result, and according to kinematic wave theory, a shock is produced between states A and U which travels at the speed s_{AU} shown in the figure. That the speed s_{AU} is positive means that the flow in state A tends to be lower than in state U because of the large spacings mentioned earlier. After the first shock, the process starts over leading to periodic oscillations moving downstream.

We also notice that in Fig. 10 (c) and (d), there is a slight difference in terms of vehicle spacings. But what is important here is that the speed-contour plots in (c) and (d) match well, which means the simulation captures the main macroscopic features of the field trajectories.

7. Discussion

This paper presents a generalization of the works conducted by Laval et al. (2014) and Yuan et al. (2018), each producing different features of traffic instabilities, by adding a dimensionless parameter m. This parameter regulates the type of driver free acceleration error on a scale from Brownian motion (BM, $m >> 1$) to geometric Brownian (g-BM, $m = 1$) acceleration processes. When $m >> 1$, this model captures proper periodicity of traffic oscillations at bottlenecks and demonstrates that human factor alone can cause traffic instabilities. This result accords with the work conducted by Laval et al. (2014) well. When $m = 1$, this model is equivalent to the model in Yuan et al. (2018), which successfully reproduces the speed-capacity relationship observed empirically.

To understand why $m >> 1$ leads to oscillations, recall that for oscillations to develop first they have to form. From equation (14 b) note that the error added to the vehicle trajectory decreases with vehicle speed. When $m = 1$ this error goes to zero when traveling at the desired speed, which prevents any initial perturbation from occurring, let alone developing into a fully grown oscillation. When $m >> 1$ the error is greater than zero and increasing with m, which allows the initial pertur-

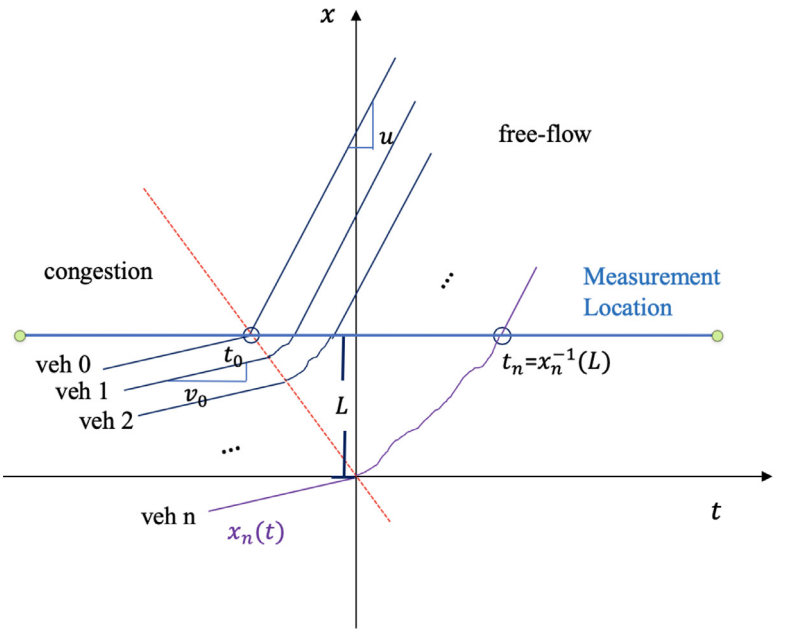

Fig. 12. The discharge flow experiment: vehicles are travelling at a constant low speed v_0 at the beginning and then accelerate to free-flow speed. The trajectory of nth vehicle $x_j(t_n)$ is shown in the figure and t_n is the time that the nth vehicle crosses the measurement location.

bation to occur (and possibly grow into a mature oscillation). To understand why $m \to 1$ leads to speed-capacity relationship in bottleneck, consider a (n+1)-vehicle car-following experiment on a one-lane road with no passing, as shown in Fig. 12. In this experiment the lead vehicle drives initially at a constant low speed v_0, then accelerates to free-flow speed in the resulting discharge rate is measured at that location $x = 0$. We can express the discharge flow as:

$$Q = \frac{n}{t_n - t_0}, \tag{18}$$

where t_n is the time that vehicle n crosses the measurement location, i.e. $x_n(t_n) = L$ which is also equal to $n\delta$ and $t_0 = -n\tau$ in our case. Using the law of total probability we can write:

$$\begin{aligned} P(x_n(t) \geq L) &= P(x_n(t) \geq L \mid t_n \leq t)P(t_n \leq t) + P(x_n(t) \geq L \mid t_n > t)P(t_n > t) \\ &= 1 \times P(t_n \leq t) + 0 \times P(t_n > t) \\ &= P(t_n \leq t). \end{aligned} \tag{19}$$

The second equality in (19) follows from $x_n(t)$ being a monotonic increasing function, and thus $x_n(t) \geq x_n(t_n) = L$ only if $t_n \leq t$. Consequently, $P(x_n(t) \geq L \mid t_n \leq t) = 1$ and $P(x_n(t) \geq L \mid t_n > t) = 0$. Combining (18) and (19) we have that the cumulative distribution function of the discharge rate Q can be written as:

$$\begin{aligned} P(Q < q) &= P\left(t_n > \frac{n}{q} + t_0\right) \\ &= P\left(x_n\left(\frac{n}{q} + t_0\right) < L\right) \\ &= 1 - \frac{1}{4}\mathrm{erfc}\left(\frac{n\delta - \mathrm{E}\left[\xi_n\left(\frac{n(1-\tau q)}{q}\right)\right]}{\sqrt{2}\mathrm{SD}\left[\xi_n\left(\frac{n(1-\tau q)}{q}\right)\right]}\right)\mathrm{erfc}\left(\frac{\delta q - u}{\sqrt{2}q\sqrt{\sigma_\delta^2 + \sigma_\tau^2 u^2}}\right) \end{aligned} \tag{20}$$

which is analytical. Fig. 13 shows the expected value of the discharge flow, $E(Q)$, against the speed in congestion for different model parameters. The left panel in the figure shows that the slope of the line decreases with m, and the model loses its ability to generate speed-capacity relationship in the Brownian motion limit. The right panel in the figure strongly suggests that the product $m \cdot \tilde{\sigma}$ is the main parameter of the model, while the bottom panel illustrates how the discharge flow decreases with $m \cdot \tilde{\sigma}$. We verified that these results hold for a wide range for the remaining parameter values. Notably, it turns out that the parameter $m \cdot \tilde{\sigma}$ is statistically the same across different experiments and different datasets; see Fig. 14.

We find that if we select $m \approx 1.2$, the model could do both the oscillation and speed-capacity relationship (Xu and Laval, 2019). In the future, we plan to do statistical tests on the model homogeneity between different drivers and different vehicle classes (regular vehicles and trucks). If we find the model parameters are not homogeneous between different

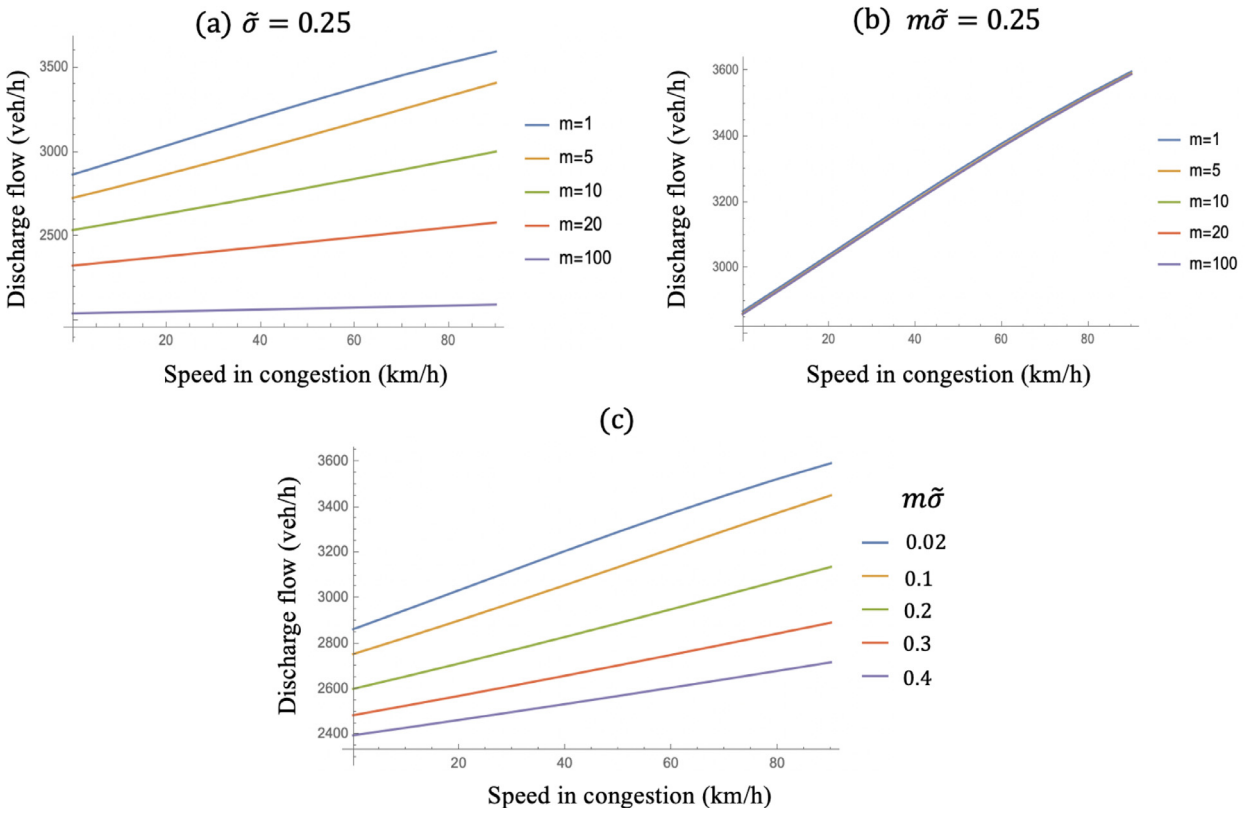

Fig. 13. The plot of discharge flow against speed in congestion. We used $n = 50$, $\mu_\delta = 6$m, $\mu_\tau = 0.75$s, $u = 100$km/h, $\beta = 200\text{h}^{-1}$, $\sigma_\delta = 1$m and $\sigma_\tau = 0.4$s.

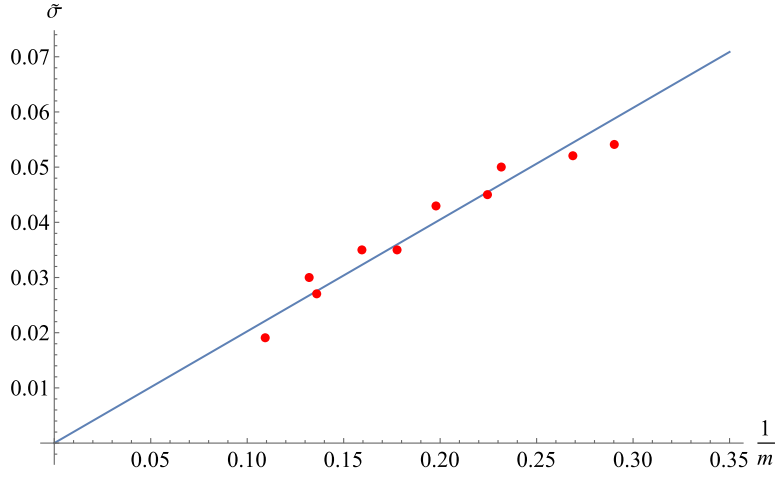

Fig. 14. This figure shows the linear relationship between $\frac{1}{m}$ and $\tilde{\sigma}$. Data are from 10 car-following experiments from two datasets. The regression result is $\tilde{\sigma} = 0.202\frac{1}{m}$. The regression coefficient R-squared is 0.994.

drivers or vehicle types, we will consider assigning different values of ms to different groups of drivers or vehicles to build hybrid models. Such hybrid models have good potential to reproduce different types of traffic instabilities.

We used MLE to estimate model parameters. Unlike existing literature that simply adds a white noise to a deterministic car-following model as in (1), the probability distribution of vehicle positions in our model is analytical, which should produce much more accurate MLE parameter estimates. As an example, take the parameters τ and δ: existing methodologies based in (1) would be unable to estimate their variances and their correlation.

Based on MLE results from the two datasets used in this paper, we were able to test different hypotheses. We found that driver acceleration is negatively correlated with grade as expected. Different from Laval et al. (2014), we find that drivers

compensate by pressing the gas harder than usual when they come to an upgrade segment. Currently, the formulation assumes a linear relationship between the desired speed and roadway upgrade for the free-flow part of the model. In the future, we plan to study the following questions: (i) this relationship may not be linear, and (ii) downgrade may also affect a driver's acceleration process. The study does not require a major change of the model. We can simply rewrite $\alpha g \max\{0, G\}$ as $gf(G)$, where $f(G)$ can be very flexible.

The data gives a strong indication that the value of m is larger than 3, which means that the acceleration processes of drivers are closer to BM than g-BM. Unfortunately, it also means that the model loses its ability to explain the speed-capacity relationship, as discussed in Section 3.2.4. This could be explained by a number of reasons and should be the focus of future research. One possibility is that controlled experiments such as the ones used here, are not representative of typical driving behavior because drivers might feel compelled to perform excessively well. This could also explain the unusually small values of τ estimated here, and also the vehicle bounces observed in Section 6, where drivers that are trailing behind feel an increased urge to catch up with the platoon. We are currently in the process of running our estimation framework on data gathered from videos of real uncontrolled traffic, and we will be able to test these hypotheses with the methods outlined here. Another possibility is that m might be different for different traffic states and vehicles have values of $m \approx 1$ when the queue is discharging. This assumption needs to be tested in the future.

We used likelihood-ratio test to find that model parameters are the same across different experiments within one dataset while they are different across different datasets. In the future, a wide variety of hypotheses might be tested by statistical inference methods, such as homogeneity of driver/vehicle population, the significance of traffic states or the impacts of environmental variables, such as weather and visibility.

Finally, we conjecture that the proposed model is well suited to represent the operations of automated vehicles. To see this, (i) manufacturers strive to implement car-following behaviors that are similar to human drivers, (ii) AVs also have to overcome gravity and are subject to limited engine power, which implies that a bounded acceleration model is in order for AVs as well, (iii) existing single-regime models for AV's can be incorporated in the congestion term in (10) by expressing them in terms of vehicle positions rather than acceleration. In the future, the impacts of AVs on this model might be tested with statistical inference methods.

Acknowledgements

We would like to thank the reviewers of this manuscript, whose comments greatly improved its quality. We will also like to thank Prof. Rui Jiang from Beijing Jiaotong University, for providing the car-the following data. This study has received funding from NSF research projects # 1562536 and # 1826003.

Appendix A

$$
\begin{aligned}
\mathrm{Var}[\xi(t)] = {} & \frac{1}{\beta^2(2\beta^2 - 3\beta\sigma^2 + \sigma^4)^2} e^{-t(\beta+\sigma^2)} (e^{t(-\beta+\sigma^2)}(-1+e^{\beta t})((v_c - v_0)^2 \\
& + e^{\beta t}((5 + 2(-4+m)m)v_c^2 + 2(-1+2m)v_c v_0 - v_0^2))\sigma^8 + 4\beta^4 e^{t(-\beta+\sigma^2)} \\
& ((-1+e^{t\sigma^2})(v_c - v_0)^2 + e^{2\beta t}(-1+m)^2 t v_c^2 \sigma^2 + 4e^{\beta t}(-1+m)t v_c(-v_c + v_0)\sigma^2 \\
& 2\beta^3 e^{-\beta t}\sigma^2 (6e^{t\sigma^2}(v_c - v_0)^2 - e^{2t\sigma^2}((2+m)v_c - 3v_0)(m v_c - v_0) + 4e^{t(\beta+\sigma^2)} \\
& (-2m v_c^2 + m^2 v_c^2 + 2v_c v_0 - v_0^2 + 4(-1+m)t v_c(v_c - v_0)\sigma^2) + e^{t(2\beta+\sigma^2)} \\
& ((2-4m)v_c v_0 + v_0^2 + v_c^2(-6 + 10m - 3m^2 - 5(-1+m)^2 t\sigma^2))) \\
& 2\beta\sigma^6 (3e^{t(-\beta+\sigma^2)}(v_c - v_0)^2 + e^{t\sigma^2}(-5v_0^2 + 2v_c v_0(1 + 4m - (-1+m)t\sigma^2) \\
& + v_c^2(8 - 18m + 5m^2 + 2(-1+m)t\sigma^2)) - e^{t(\beta+\sigma^2)}(4(-1+2m)v_c v_0 - 2v_0^2 \\
& + v_c^2(11 - 18m + 5m^2 + (-1+m)^2 t\sigma^2))) + \beta^2 e^{-\beta t}\sigma^4(-13e^{t\sigma^2}(\beta - v_0)^2 \\
& + 2e^{2t\sigma^2}(-m v_c + v_0)^2 - 4e^{t(\beta+\sigma^2)}(4e^{t(\beta+\sigma^2)}(4(1 + (-3+m)m)v_c^2 \\
& + 4(1+m)v_c v_0 - 4v_0^2 + 5(-1+m)t v_c(v_c - v_0)\sigma^2) + e^{t(2\beta+\sigma^2)}(10(-1+2m)v_c v_0 \\
& - 5v_0^2 + v_c^2(29 - 48m + 14m^2 + 8(-1+m)^2 t\sigma^2))))
\end{aligned}
$$

Appendix B. MLE

We use MLE for the estimation of parameters in our proposed model. In a nutshell, MLE consists in finding the value of Θ that maximize the log-likelihood $\ell(\mathbf{x}; \Theta) = \sum_{i,j} \ln[f(x_j(t_i); \Theta)]$.

This gives the MLE estimator of Θ, and is denoted $\widehat{\Theta}$. MLE is appealing because for large samples one can perform statistical inference analysis to answer important questions in car-following behavior. For large samples the distribution of MLE estimators tends to the multivariate normal distribution, i.e. $\widehat{\Theta} \overset{dist}{\to} N(\Theta, \mathrm{SD}[\Theta])$, where the covariance matrix $\mathrm{SD}[\Theta]$

can be approximated using the Cramer-Rao lower bound: $SD[\Theta] \approx J(\widehat{\Theta})^{-1}$ where $J(\Theta) = -\frac{\partial^2 \ell(\Theta)}{\partial \Theta^2}$ is the observed Fisher's information for the sample. This important result allows us to use the statistical inference toolbox, in particular confidence intervals and hypothesis testing.

A likelihood-ratio test can be used to compare the goodness-of-fit of different model specifications. For example, if we have two models with number of parameters n_1 and n_2 $(n_1 > n_2)$, respectively, the likelihood-ratio test statistic is $\Lambda(\mathbf{x}) = 2\left[\ell(\mathbf{x}; \widehat{\Theta_1}) - \ell(\mathbf{x}, \widehat{\Theta_2})\right]$ which follows a chi-square distribution with $n_1 - n_2$ degrees of freedom. For more information on MLE, the reader is referred to Hubbert (2012).

References

Ahmed, K.I., 1999. Modeling Driver's Acceleration and Lane Changing Behavior Ph.D. thesis.

Ahn, S., Cassidy, M., 2007. Freeway traffic oscillations and vehicle lane-change manoeuvres. In: Heydecker, B., Bell, M., Allsop, R. (Eds.), 17th International Symposium on Transportation and Traffic Theory. Elsevier, New York, pp. 691–710.

Ahn, S., Cassidy, M., Laval, J.A., 2003. Verification of a simplified car-following theory. Transp. Res. Part B 38 (5), 431–440.

Ahn, S., Vadlamani, S., Laval, J., 2013. A method to account for non-steady state conditions in measuring traffic hysteresis. Transp. Res. Part C (34) 138–147. doi:10.1016/j.trc.2011.05.020.

Ang, A.H., Tang, W., 2007. Probability Concepts in Engineering, second John Wiley & Sons.

Bilbao-Ubillos, J., 2008. The costs of urban congestion: Estimation of welfare losses arising from congestion on cross-town link roads. Transp. Res. Part A 42 (8), 1098–1108.

Chen, D., Laval, J., Zheng, Z., Ahn, S., 2012. A behavioral car-following model that captures traffic oscillations. Transp. Res. Part B 46 (6), 744–761. doi:10.1016/j.trb.2012.01.009.

Chen, D., Laval, J.A., Ahn, S., Zheng, Z., 2012. Microscopic traffic hysteresis in traffic oscillations: a behavioral perspective. Transp. Res. Part B 46 (10), 1440–1453. doi:10.1016/j.trb.2012.07.002.

Hoogendoorn, S., Ossen, S., 2005. Parameter estimation and analysis of car-following models. Transp. Traffic Theory 245–265.

Hubbert, S., 2012. Essential Mathematics for market risk management, 2nd John Wiley & Sons.

Jiang, R., Hu, M.-B., Zhang, H.M., Gao, Z.-Y., Jia, B., Wu, Q.-S., Wang, B., Yang, M., 2014. Traffic experiment reveals the nature of car-following. PLOS ONE 9 (4), 1–9.

Kim, K., Cassidy, M.J., 2012. A capacity-increasing mechanism in freeway traffic. Transp. Res. Part B 46 (9), 1260–1272. doi:10.1016/j.trb.2012.06.002.

Laval, J.A., 2005. Linking synchronized flow and kinematic wave theory. In: Schadschneider, A., Poschel, T., Kuhne, R., Schreckenberg, M., Wolf, D. (Eds.), Traffic and Granular Flow '05. Springer. 521–526.

Laval, J.A., 2011. Hysteresis in traffic flow revisited: an improved measurement method. Transp. Res. Part B 45 (2), 385–391. doi:10.1016/j.trb.2010.07.006.

Laval, J.A., Daganzo, C.F., 2006. Lane-changing in traffic streams. Transp. Res. Part B 40 (3), 251–264.

Laval, J.A., Leclercq, L., 2008. Microscopic modeling of the relaxation phenomenon using a macroscopic lane-changing model. Transp. Res. Part B 42 (6), 511–522. doi:10.1016/j.trb.2007.10.004.

Laval, J.A., Leclercq, L., 2010. A mechanism to describe the formation and propagation of stop-and-go waves in congested freeway traffic. Philos. Trans. R. Soc. A 368 (1928), 4519–4541.

Laval, J.A., Toth, C.S., Zhou, Y., 2014. A parsimonious model for the formation of oscillations in car-following models. Transp. Res. Part B 70, 228–238.

Leclercq, L., Chiabaut, N., Laval, J., Buisson, C., 2007. Relaxation phenomenon after changing lanes: Experimental validation with NGSIM data set. Transp. Res. Rec. 1999, 79–85.

Leclercq, L., Laval, J.A., 2007. A multiclass car-following rule based on the "lighthill-whitham-richards" model. In: Appert-Rolland, C., Lassarr, S., Gondret, P., Dauchot, O., Sykes, C. (Eds.), Traffic and Granular Flow '07 (Forthcoming). Springer.

Leclercq, L., Laval, J.A., Chiabaut, N., 2011. Capacity drops at merges: an endogenous model. Procedia - Social Behav. Sci. 17 (0), 12–26. doi:10.1016/j.sbspro.2011.04.505. Papers selected for the 19th International Symposium on Transportation and Traffic Theory.

Mauch, M., Cassidy, M. J., 2002. Freeway traffic oscillations: Observations and predictions. In: Taylor, M. (Ed.), 15th Int. Symp. on Transportation and Traffic Theory. Pergamon-Elsevier, Oxford, U.K.

Nadarajah, S., Kotz, S., 2008. Exact distribution of the max/min of two gaussian random variables. IEEE Trans. Very Large Scale Integr.(VLSI) Syst. 210–212.

Newell, G.F., 2002. A simplified car-following theory : a lower order model. Transp. Res. Part B 36 (3), 195–205.

Sugiyama, Y., Fukui, M., Kikuchi, M., Hasebe, K., Nakayama, A., Nishinari, K., Tadaki, S.-i., Yukawa, S., 2008. Traffic jams without bottlenecks-experimental evidence for the physical mechanism of the formation of a jam. New J. Phys. 10, 033001.

Treiber, M., Hennecke, A., Helbing, D., 1999. Derivation, properties, and simulation of a gas-kinetic-based, non-local traffic model. Phys. Rev. E 59, 239.

Treiber, M., Kesting, A., 2012. Validation of traffic flow models with respect to the spatiotemporal evolution of congested traffic patterns. Transp. Res. Part C 21 (1), 31–41. doi:10.1016/j.trc.2011.09.002.

Treiber, M., Kesting, A., 2017. The intelligent driver model with stochasticity -new insights into traffic flow oscillations. Transp. Res. Procedia 23 (Supplement C), 174–187. Papers Selected for the 22nd International Symposium on Transportation and Traffic Theory Chicago, Illinois, USA, 24-26 July, 2017.

Treiterer, J., Myers, J.A., 1974. The hysteresis phenomenon in traffic flow. In: Buckley, D.J. (Ed.), 6th Int. Symp. on Transportation and Traffic Theory. A.H. and A.W. Reed, London. 13–38.

Wilson, R., Ward, J., 2011. Car-following models: fifty years of linear stability analysis - a mathematical perspective. Transp. Plann. Technol. 34 (1), 3–18. doi:10.1080/03081060.2011.530826.

Wilson, R.E., 2008. Mechanisms for spatio-temporal pattern formation in highway traffic models. Phil. Trans. R. Soc. A 1872, 2017–2032.

Xu, T., Laval, J., 2019. Analysis of a two-regime stochastic car-following model: explaining capacity drop and oscillation instabilities. Transp. Res. Rec.. Accepted.

Yuan, K., Knoop, V.L., Hoogendoorn, S.P., 2015. Capacity drop: Relationship between speed in congestion and the queue discharge rate. Transp. Res. Rec. 2491, 72–80. doi:10.3141/2491-08.

Yuan, K., Laval, J., Knoop, V.L., Jiang, R., Hoogendoorn, S., 2018. A geometric brownian motion car-following model: towards a better understanding of capacity drop. Transportmetrica B. Forthcoming.

Zheng, Z., Ahn, S., Chen, D., Laval, J., 2011. Applications of wavelet transform for analysis of freeway traffic: bottlenecks, transient traffic, and traffic oscillations. Transp. Res. Part B 45 (2), 372–384. doi:10.1016/j.trb.2010.08.002.

Zheng, Z., Ahn, S., Monsere, C.M., 2010. Impact of traffic oscillations on freeway crash occurrences. Accid. Anal. Prevent. 42 (2), 626–636.